

SEONG-HO HA<sup>1\*</sup>, YOUNG-CHUL SHIN<sup>1</sup>, BONG-HWAN KIM<sup>1</sup>, YOUNG-OK YOON<sup>1</sup>,  
HYUN-KYU LIM<sup>1</sup>, SUNG-HWAN LIM<sup>2</sup>, SHAE K. KIM<sup>1</sup>

## CHARACTERIZATION OF Ca PRECIPITATION IN Al-Mg ALLOYS CONTAINING A TRACE OF Ca DURING HOMOGENIZATION

In this study, precipitation of Ca in Al-Mg alloys containing a trace of Ca during homogenization was investigated using a transmission electron microscope (TEM) and calculated phase diagrams. TEM result indicated that the Ca-based particles found in the examined sample are  $\text{Ca}_7\text{Mg}_{7.5}\text{Si}_{14}$ . From the calculation of Scheil-Gulliver cooling, it was found that the Ca was formed as  $\text{Al}_4\text{Ca}$  and C36 laves phases with  $\text{Mg}_2\text{Si}$  and  $\text{Al}_{13}\text{Fe}_4$  from other impurities phase during solidification. No Ca-Mg-Si ternary phase existed at the homogenization temperature in the calculated phase diagram. From the phase diagram of Al- $\text{Al}_4\text{Ca}$ - $\text{Mg}_2\text{Si}$  three-phase isothermal at 490°C, it was shown that  $\text{Ca}_7\text{Mg}_6\text{Si}_{14}$  phase co-exists with Al,  $\text{Mg}_2\text{Si}$  and  $\text{Al}_4\text{Ca}$  in the largest region and with only Al and  $\text{Mg}_2\text{Si}$  in  $\text{Al}_4\text{Ca}$ -poor regions. It was thought that the  $\text{Ca}_7\text{Mg}_6\text{Si}_{14}$  ternary phase was formed by the interaction between  $\text{Mg}_2\text{Si}$  and  $\text{Al}_4\text{Ca}$  considering that the segregation can occur throughout the entire microstructures.

*Keywords:* Al-Mg system, precipitation, Mg+ $\text{Al}_2\text{Ca}$  master alloy, Transmission electron microscope, Phase diagram

### 1. Introduction

Al-Mg alloys are increasingly used due to the excellent corrosion resistance, weldability, and formability [1]. The need to increase Mg over 5wt% in Al alloys has grown due to their high tensile and fatigue strength and better weldability. On the other hand, the enrichment of Mg content over 5wt% is limited because of the strong affinity to oxygen, leading to the formation of Mg oxides dross and inclusions during the melting, holding and casting processes [2-5]. It was reported that addition of a small amount of Ca is one of the ways to reduce Mg oxidation during melt process [6-8]. The Ca near the surface is consumed to make an oxide film and protect the melt during melting process, while it forms intermetallic compounds during solidification due to its limited solubility in solid state [9]. The Ca-based intermetallic compounds are possibly precipitated by heat treatments such as homogenization and annealing at high temperatures. The distribution of Ca-based phases plays an important role in controlling the preferential oxidation of  $\beta\text{-Al}_3\text{Mg}_2$  eutectic phase, which begins at grain boundaries [3]. Precipitation of Ca-containing phases can occur by the interactions with other impurities in Al alloys. In this study, precipitation of Ca in Al-Mg alloys containing a trace of Ca during homogenization was investigated. The

precipitates in the samples were examined using a transmission electron microscope and also discussed based on the phase diagrams calculated thermodynamically in this study.

### 2. Experimental

The experimental material examined in this work is Al-6 mass%Mg based alloy (as-received) whose analyzed composition is given in Table 1. As a billet for extrusion, the examined Al alloy whose composition is Mg: 6.22 mass%, Si: 0.06 mass%, Fe: 0.07 mass%, Ti: 0.03 mass%, and Al and other impurities: Bal. was used. Mg+ $\text{Al}_2\text{Ca}$  master alloy was used for a simultaneous addition of Mg and a trace of Ca [8] in the melting and alloying processes. The exact amount of Ca cannot be provided in this study because it is regarded as a confidential information, but is shown as approximately 0.1 mass%. Homogenization at 490°C for 8 h is done on the alloy. The Ca-based phases in the samples were observed using a 200-kV field-emission transmission electron microscope (JEOL-2100F, JEOL, Japan) equipped with an energy-dispersive X-ray spectroscopy (EDS) detector. The TEM specimens were prepared as 3-mm-diameter, 100-mm-thick disk-type plates via mechanical polishing with a digitally

<sup>1</sup> KOREA INSTITUTE OF INDUSTRIAL TECHNOLOGY (KITECH), INCHEON 21999, REPUBLIC OF KOREA

<sup>2</sup> KANGWON NATIONAL UNIVERSITY, DEPARTMENT OF ADVANCED MATERIALS SCIENCE AND ENGINEERING, CHUNCHEON 24341, REPUBLIC OF KOREA

\* Corresponding author: seonghoha1999@gmail.com



enhanced precision specimen grinder (DEPS-101). Before being inserted into the TEM chamber, the specimens were trimmed and cleaned by precision ion polishing with a 691 PIPS device (Gatan) and subjected to plasma cleaning with a Fischione 1020 cleaner. The formation of Ca-based phases during solidification and homogenization were also examined based on the phase diagrams calculated by *FactSage 7.3* [10], a thermodynamic software package.

### 3. Results and discussion

Fig. 1 presents TEM analysis of Ca-based precipitations found in the sample. Bright-field TEM images of the analyzed area are given in Fig. 1(a) and (b). The particle analyzed seems to be comprised of two phases. The compositions analyzed by EDS for areas numbered as 1, 2, and 3 as shown in Fig. 1(b) are given in Table 1. Based on the compositional information, Area 3 appears to correspond to the matrix. High resolution images of the analyzed particles and digital diffractograms obtained by a fast Fourier transform (FFT) (inset of Fig. 1(c)) are shown in Fig. 1(c) and (d). From those results, the analyzed particles are found to be  $\text{Mg}_2\text{Si}$  and  $\text{Ca}_7\text{Mg}_{7.5}\text{Si}_{14}$  phases, respectively.

TEM results of other particles found in the sample are presented in Fig. 2. Based on the compositional data shown in Table 1 and digital diffractogram obtained by FFT, the analyzed Ca-bearing particle was found to be  $\text{Ca}_7\text{Mg}_{7.5}\text{Si}_{14}$  phase, which is in a good agreement with that in Fig. 1. A relatively coarse particle was also observed near the  $\text{Ca}_7\text{Mg}_{7.5}\text{Si}_{14}$  phase and defined as  $\text{Al}_3\text{Fe}_3$  phase considered to be formed by Fe impurity based on the composition and diffractogram obtained by FFT.

TABLE 1

Analyzed compositions of numbered areas shown in Fig. 1 and 2 by EDS

Area	Analyzed composition (at%)					
	Al	Mg	Si	Fe	Ca	Other impurity elements
1	41.46	18.54	18.3	—	16.56	Bal.
2	4.07	60.97	31.63	—	—	Bal.
3	90.02	6.74	—	—	—	Bal.
4	39.99	16.11	14.84	—	23.6	Bal.
5	78.87	—	—	17.93	—	Bal.

In order to predict the present Ca-based phases before the homogenization, the formation of secondary particles during so-

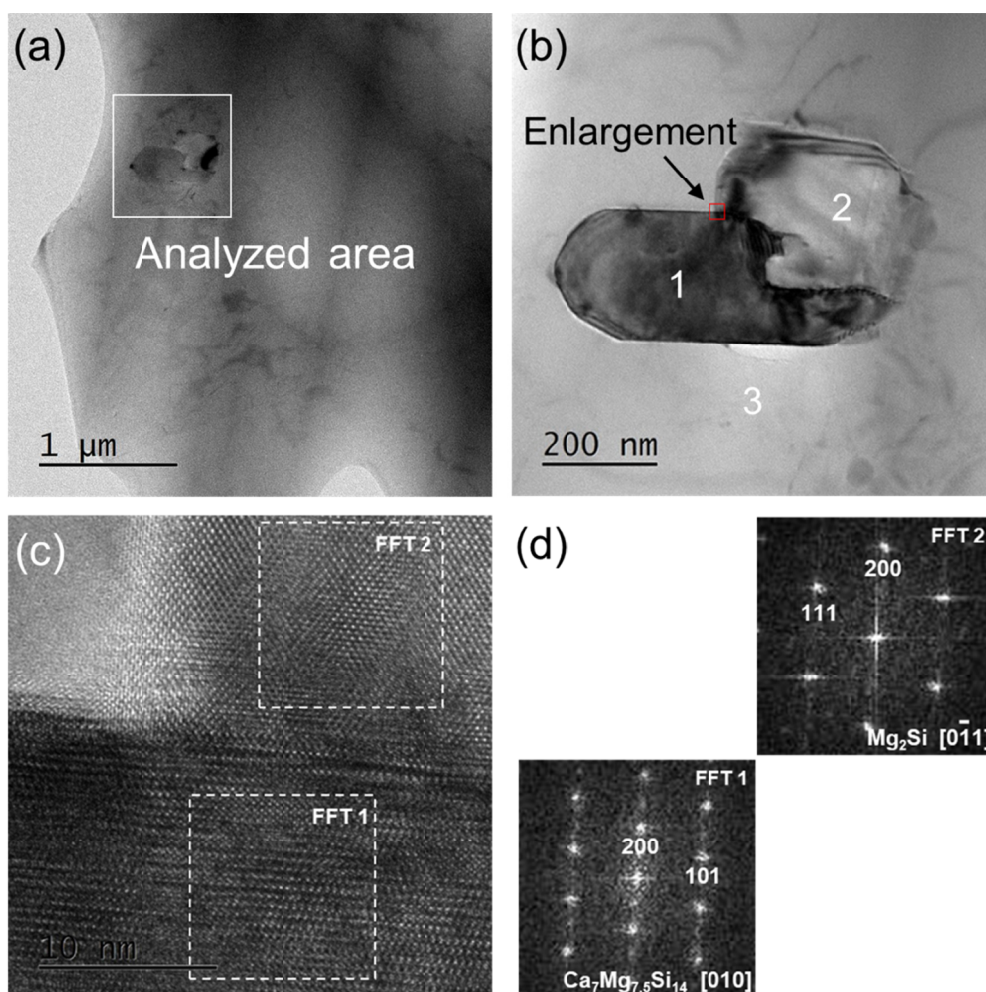


Fig. 1. (a) Bright-field TEM image of analyzed area, (b) enlargement of the analyzed area, (c) high-resolution image (marked with solid line in (b)), and (d) digital diffractogram obtained by FFT (inset of (c))

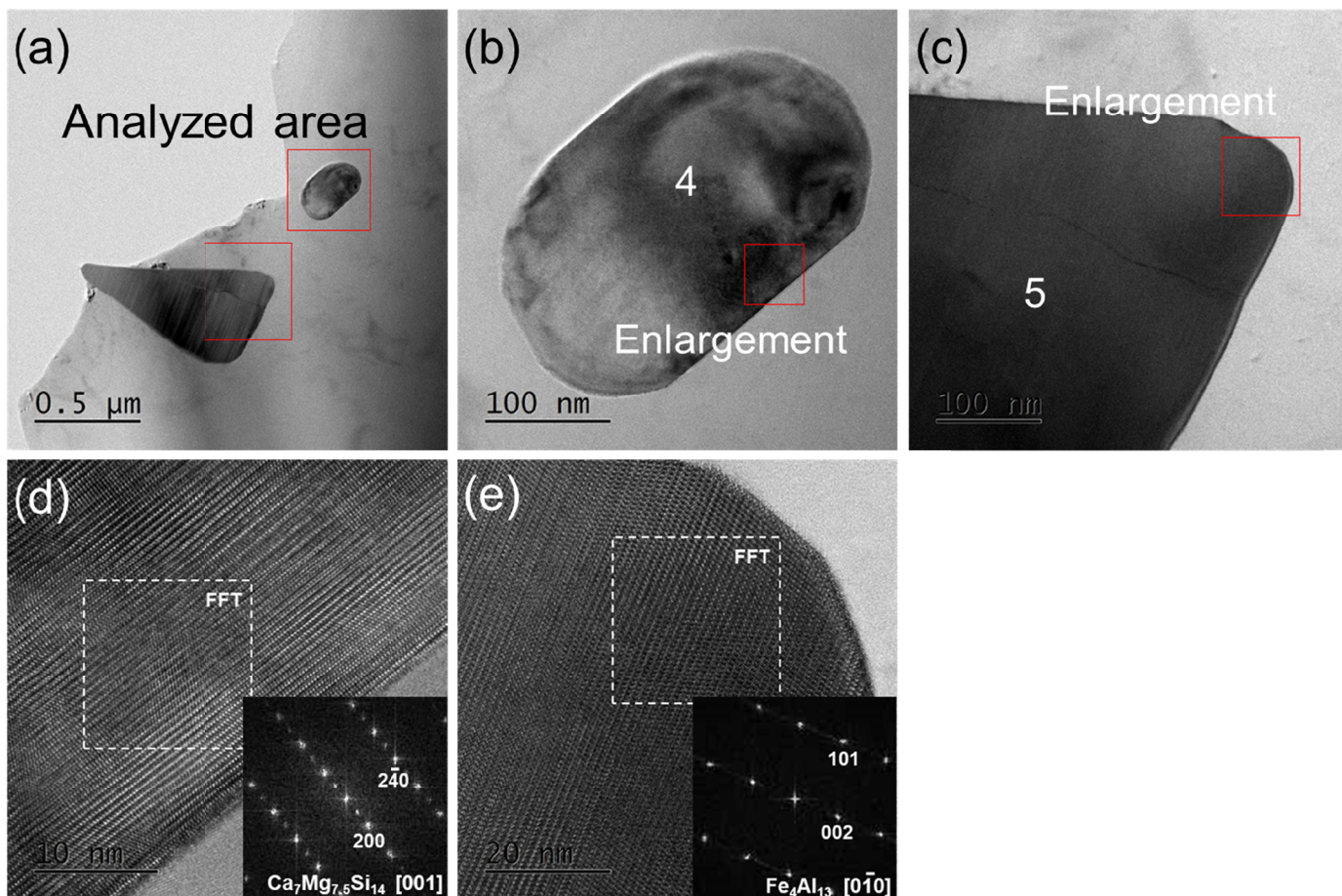


Fig. 2. (a) Bright-field TEM image of analyzed area, (b, c) enlargement of analyzed area, (d, e) high-resolution images marked with solid line in (b) and (c), respectively, and digital diffractograms obtained by FFT

olidification was examined via Scheil-Gulliver cooling calculated by *FactSage 7.3*. The solidification sequence of the examined alloy based on Scheil-Gulliver cooling calculation is as follows:

Constituent 1	$L \rightarrow Al$
Constituent 2	$L \rightarrow Al + Al_{13}Fe_4$
Constituent 3	$L \rightarrow Al + Mg_2Si + Al_{13}Fe_4$
Constituent 4	$L \rightarrow Al + Mg_2Si + Al_4Ca + Al_{13}Fe_4$
Constituent 5	$L \rightarrow Al + Mg_2Si + C36 + Al_{13}Fe_4$
Constituent 6	$L \rightarrow Al + Mg_2Si + C36 + Al_{13}Fe_4 + \beta-Al_3Mg_2$

As shown above, there are various eutectic reactions including the phases from the alloying elements and impurities. It is confirmed that  $Mg_2Si$  and  $Al_{13}Fe_4$  phases observed in Fig. 1 and 2 are possibly present in as-cast alloy. During the solidification, the Ca is formed as two phases;  $Al_4Ca$  and C36 laves phase. Moreover, both Ca-based phases can co-exist with  $Mg_2Si$  at the grain boundaries. Therefore, the interaction between Ca-based and  $Mg_2Si$  phases can occur during the homogenization.

As can be seen in Fig. 3, the phase diagram plotted for Si versus Ca mass fractions at  $490^\circ C$  calculated by *FactSage 7.3* was examined to predict the stable phases and potential precipitates newly formed at the homogenization conditions. At the given temperature and throughout the entire compositional ranges,  $Al_4Ca$  and  $Al_{13}Fe_4$  are stable phases, indicating that

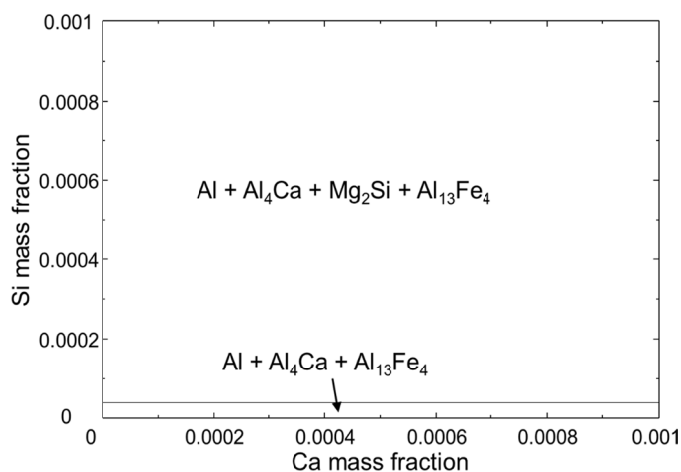


Fig. 3. Phase diagram plotted for Si versus Ca mass fractions at  $490^\circ C$  calculated by *FactSage 7.3*. The contents of Mg and Fe are fixed at those mentioned in the section of Experimental

these elements are rarely soluble in the Al matrix. The  $Mg_2Si$  is also present in the most of the compositional ranges. Therefore,  $Mg_2Si$ ,  $Al_{13}Fe_4$ , and  $Al_4Ca$  phases should be found if the alloy reached equilibrium at  $490^\circ C$ . The presence of  $Mg_2Si$  and  $Al_{13}Fe_4$  phases is in a good agreement with the results from TEM analysis. On the other hand, no Ca-Mg-Si ternary

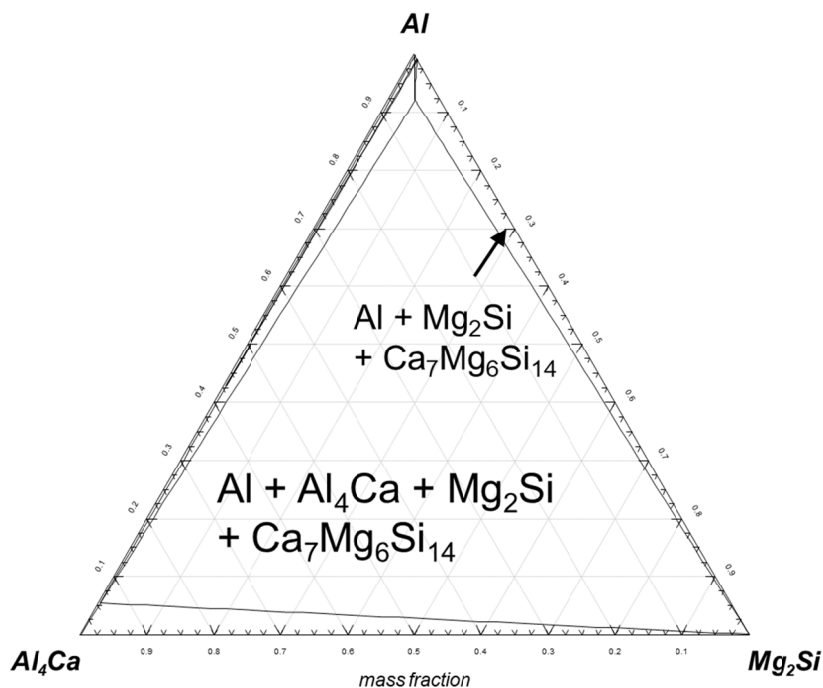


Fig. 4. Phase diagram of Al-Al<sub>4</sub>Ca-Mg<sub>2</sub>Si three-phase system isothermal at 490°C calculated by *FactSage 7.3*

phase can exist in both before and after the homogenization only based on the thermodynamic calculation aforementioned. Therefore, the another calculation was done on the phase diagram of Al-Al<sub>4</sub>Ca-Mg<sub>2</sub>Si three-phases at 490°C as shown in Fig. 4 to predict inter-products among the three phases. Ca<sub>7</sub>Mg<sub>6</sub>Si<sub>14</sub> phase co-exists with Al, Mg<sub>2</sub>Si and Al<sub>4</sub>Ca in the largest region and with only Al and Mg<sub>2</sub>Si in Al<sub>4</sub>Ca-poor regions. Therefore, it is considered that the Ca<sub>7</sub>Mg<sub>6</sub>Si<sub>14</sub> ternary phase is formed by the interaction between Mg<sub>2</sub>Si and Al<sub>4</sub>Ca. However, the alloy examined in this study contains only trace amounts of Si and Ca and consequently, its composition is not included in the regions with Ca<sub>7</sub>Mg<sub>6</sub>Si<sub>14</sub> phase aforementioned. Considering that the segregation can occur depending on the microstructures, on the other hand, the Ca<sub>7</sub>Mg<sub>6</sub>Si<sub>14</sub> ternary phase might be formed by the interaction between Al<sub>4</sub>Ca and Mg<sub>2</sub>Si during the homogenization. The ternary phase defined in the TEM analysis mentioned above has a slightly different formula with that in the phase diagrams. They are possibly different depending on the data base of compounds. And also, the formulas in phase diagrams can change considering that the diffusions of constituent elements and presence of vacancies are not examined in thermodynamics.

#### 4. Conclusions

TEM results on the examined alloy sample showed the existence of Mg<sub>2</sub>Si and Al<sub>13</sub>Fe<sub>4</sub> from impurities and Ca<sub>7</sub>Mg<sub>7.5</sub>Si<sub>14</sub> as Ca-based phase. As a result of the calculation of Scheil-Gulliver cooling, it was found that the Ca was formed as Al<sub>4</sub>Ca and C36 laves phase during solidification. No Ca-Mg-Si ternary phase was stable at the homogenization temperature and given alloy composition in the calculated phase diagram. On the other

hand, from the phase diagram of Al-Al<sub>4</sub>Ca-Mg<sub>2</sub>Si three-phase isothermal at 490°C, it was shown that Ca<sub>7</sub>Mg<sub>6</sub>Si<sub>14</sub> phase co-exists with Al, Mg<sub>2</sub>Si and Al<sub>4</sub>Ca in the largest region. Due to trace amounts of Si and Ca contained in the examined alloy, the alloy composition is not included in the regions with Ca<sub>7</sub>Mg<sub>6</sub>Si<sub>14</sub> phase. Considering that the segregation can occur depending on the microstructures, on the other hand, the Ca<sub>7</sub>Mg<sub>6</sub>Si<sub>14</sub> ternary phase is possibly formed by the interaction between Al<sub>4</sub>Ca and Mg<sub>2</sub>Si during the homogenization.

#### REFERENCES

- [1] J.R. Davis, ASM International, Aluminum and Aluminum Alloys, Materials Park 1993.
- [2] G. Wu, K. Dash, M.L. Galano, K.A.Q. O'Reilly, *Corros. Sci.* **155**, 97 (2019).
- [3] B.H. Kim, S.H. Ha, Y.O. Yoon, H.K. Lim, S.K. Kim, D.H. Kim, *Mater. Lett.* **228**, 108 (2018).
- [4] S.H. Ha, B.H. Kim, Y.O. Yoon, H.K. Lim, T.W. Lee, S.H. Lim, S.K. Kim, *Sci. Adv. Mater.* **10**, 697 (2018).
- [5] D. Ajmera, E. Panda, *Corros. Sci.* **102**, 425 (2016).
- [6] S.H. Ha, J.K. Lee, S.K. Kim, *Mater. Trans.* **49**, 1081 (2008).
- [7] S.H. Ha, B.H. Kim, Y.O. Yoon, H.K. Lim, T.W. Lee, S.H. Lim, S.K. Kim, *Int. J. Metalcast.* **13**, 121 (2019).
- [8] J.W. Jeong, J.S. Im, K. Song, M.H. Kwon, S.K. Kim, Y.B. Kang, S.H. Oh, *Acta Mater.* **61**, 3267 (2013).
- [9] K. Ozturk, L.Q. Chen, Z.K. Liu, *J. Alloys Compd.* **340**, 199 (2002).
- [10] C.W. Bale, E. Bélisle, P. Chartrand, S.A. Decterov, G. Eriksson, A.E. Gheribi, K. Hack, I.H. Jung, Y.B. Kang, J. Melançon, A.D. Pelton, S. Petersen, C. Robelin, J. Sangster, P. Spencer, M.A. Van Ende, *Calphad* **54**, 35 (2016).